PNAS RESEARCH ARTICLE | NEUROSCIENCE OPEN ACCESS

Highly specific σ_2R/TMEM97 ligand FEM-1689 alleviates neuropathic pain and inhibits the integrated stress response

Muhammad Saad Yousuf[a,b], James J. Sahn[b,c], Hongfen Yang[c], Eric T. David[a], Stephanie Shiers[a], Marisol Mancilla Moreno[a], Jonathan Iketem[a], Danielle M. Royer[a], Chelsea D. Garcia[a], Jennifer Zhang[a], Veronica M. Hong[a], Subhaan M. Mian[a], Ayesha Ahmad[a], Benedict J. Kolber[a], Daniel J. Liebl[d], Stephen F. Martin[b,c,1], and Theodore J. Price[a,b,1]

Edited by Allan Basbaum, University of California, San Francisco, CA; received April 14, 2023; accepted November 21, 2023

The sigma 2 receptor (σ_2R) was described pharmacologically more than three decades ago, but its molecular identity remained obscure until recently when it was identified as transmembrane protein 97 (TMEM97). We and others have shown that σ_2R/TMEM97 ligands alleviate mechanical hypersensitivity in mouse neuropathic pain models with a time course wherein maximal antinociceptive effect is approximately 24 h following dosing. We sought to understand this unique antineuropathic pain effect by addressing two key questions: do these σ_2R/TMEM97 compounds act selectively via the receptor, and what is their downstream mechanism on nociceptive neurons? Using male and female conventional knockout mice for *Tmem97*, we find that a σ_2R/TMEM97 binding compound, FEM-1689, requires the presence of the gene to produce antinociception in the spared nerve injury model in mice. Using primary mouse dorsal root ganglion neurons, we demonstrate that FEM-1689 inhibits the integrated stress response (ISR) and promotes neurite outgrowth via a σ_2R/TMEM97-specific action. We extend the clinical translational value of these findings by showing that FEM-1689 reduces ISR and p-eIF2α levels in human sensory neurons and that it alleviates the pathogenic engagement of ISR by methylglyoxal. We also demonstrate that σ_2R/TMEM97 is expressed in human nociceptors and satellite glial cells. These results validate σ_2R/TMEM97 as a promising target for further development for the treatment of neuropathic pain.

sigma 2 receptor | TMEM97 | pain | ISR | drug discovery

Significance

Neuropathic pain is a major medical problem that is poorly treated with existing therapeutics. Our findings demonstrate that targeting σ_2R/TMEM97 with a modulator reduces pain hypersensitivity in a mouse model with exquisite selectivity. We also identify integrated stress response (ISR) inhibition as a potential mechanism of action that links the receptor to cellular signaling events that have preclinical and clinical validation for pain relief. Our work suggests that σ_2R/TMEM97 can be selectively engaged by specific small molecules to produce ISR inhibition in a subset of cells that are critical for neuropathic pain. σ_2R/TMEM97-targeted therapeutics thus have the potential to offer effective pain relief without engagement of opioid receptors.

Neuropathic pain, which is caused by an injury or disease of the somatosensory nervous system, affects approximately 10% of the population and is the leading cause of high-impact chronic pain (1). Management of neuropathic pain is a major clinical challenge because available drugs not only have limited efficacy, but they also elicit serious side effects. There is a significant need for novel drugs that alleviate neuropathic pain through nonopioid and nonaddicting mechanisms and have improved side effect profiles.

The sigma 2 receptor (σ_2R) was identified in 2017 as transmembrane protein 97 (TMEM97) (2). We found that several small molecules that bind selectively to σ_2R/TMEM97 produce strong and long-lasting antineuropathic pain effects from spared nerve injury (SNI) in mice (3), a finding that was independently replicated with structurally distinct molecules (4). Although the biological function of σ_2R/TMEM97 is not well understood, it is a transmembrane protein that is associated with the endoplasmic reticulum (ER) and plays a role in calcium signaling (5, 6) and cholesterol trafficking and homeostasis (7–11). 20(*S*)-Hydroxycholesterol was recently identified as an endogenous ligand for σ_2R/TMEM97 (12). The role of σ_2R/TMEM97 in disease pathology has historically been focused on cancer (13), but it is also implicated in neurodegenerative diseases including Alzheimer's disease (14–17) and Parkinson's disease (18). Pharmacological targeting of σ_2R/TMEM97 has neuroprotective effects in a number of models of neurodegenerative conditions, including traumatic brain injury (19), Huntington's disease (20), and retinal ganglion cell degeneration (21).

The mechanism by which modulation of σ_2R/TMEM97 alleviates neuropathic pain is not known. Given the localization of σ_2R/TMEM97 at the ER, a primary hypothesis tested in our work is whether σ_2R/TMEM97 targeting may reduce pain via interference with the integrated stress response (ISR), which includes ER stress. The ISR is an adaptive response to cellular stressors such as accumulation of misfolded proteins, lipid and oxidative stress, amino acid and heme deprivation, and viral infection (22, 23). A canonical signaling event associated with the ISR is phosphorylation of eukaryotic initiation factor 2α (eIF2α) in response to cellular stress conveyed by four kinases: protein kinase R (PKR), PKR-like ER kinase (10), heme-regulated inhibitor (HRI), and general control nonderepressible 2 (GCN2). Phosphorylation of eIF2α inhibits global protein synthesis and promotes the translation of mRNAs such as activated transcription factor 4 (ATF4). We and

Author contributions: M.S.Y., J.J.S., B.J.K., S.F.M., and T.J.P. designed research; M.S.Y., H.Y., E.T.D., S.S., M.M.M., J.I., D.M.R., C.D.G., J.Z., V.M.H., S.M.M., and A.A. performed research; J.J.S., H.Y., D.J.L., and S.F.M. contributed new reagents/analytic tools; M.S.Y., J.J.S., S.S., M.M.M., J.I., D.M.R., C.D.G., J.Z., V.M.H., S.M.M., and A.A. analyzed data; and M.S.Y. and T.J.P. wrote the paper.

Competing interest statement: M.S.Y., J.J.S., S.F.M., and T.J.P. are co-founders of NuvoNuro, Inc. S.F.M. and J.J.S. report being co-inventors on patents and pending patent applications related to work described in this article.

This article is a PNAS Direct Submission.

Copyright © 2023 the Author(s). Published by PNAS. This open access article is distributed under Creative Commons Attribution License 4.0 (CC BY).

[1]To whom correspondence may be addressed. Email: sfmartin@mail.utexas.edu or Theodore.price@utdallas.edu.

This article contains supporting information online at https://www.pnas.org/lookup/suppl/doi:10.1073/pnas.2306090120/-/DCSupplemental.

Published December 20, 2023.

Downloaded from https://www.pnas.org by UNIVERSITY OF TEXAS AT DALLAS LIBRARY SERIALS on January 6, 2024 from IP address 129.110.241.53.

others have demonstrated that the induction of the ISR is associated with neuropathic pain caused by traumatic nerve injury (24, 25), metabolic disorders (26–28), and autoimmune disorders (29–31).

Another key question is whether the antineuropathic pain effects of σ_2R/TMEM97 ligands are specifically due to their binding to σ_2R/TMEM97 because such compounds can also have substantial activity at the sigma 1 receptor (σ_1R), a receptor that also promotes antinociception in animal models (32–35). We used a knockout (KO) mouse of the *Tmem97* gene, and a small molecule, FEM-1689, that has improved selectivity for σ_2R/TMEM97 to test the hypothesis that σ_2R/TMEM97 is causatively linked to antinociception in mouse neuropathic pain models. Indeed, the antinociceptive effect of FEM-1689 in the SNI model is completely absent in TMEM97KO mice. Our findings also show that FEM-1689 inhibits the ISR in a σ_2R/TMEM97-dependent fashion in mouse and human DRG neurons. This work provides a strong mechanistic case for targeting of σ_2R/TMEM97 as the basis of an approach to treat neuropathic pain.

Results

TMEM97 mRNA Is Expressed in the Human and Mouse Dorsal Root Ganglia. To assess whether σ_2R/TMEM97 is expressed in human nociceptors, we performed RNAscope in situ hybridization using human dorsal root ganglia (DRG) obtained from organ donors. We found that *TMEM97* is expressed in all classes of human sensory neurons including *SCN10A* (Nav1.8)-positive, putative nociceptors (Fig. 1 *A*–*C*). Approximately 70% of all human DRG neurons expressed *SCN10A* transcripts, consistent with our previous observations (36), and all neurons evaluated expressed *TMEM97* mRNA (Fig. 1*C*). Cell size distribution matrix of *TMEM97* expressing neurons (average = 74 μm) showed that *TMEM97* mRNA was not restricted to a subpopulation

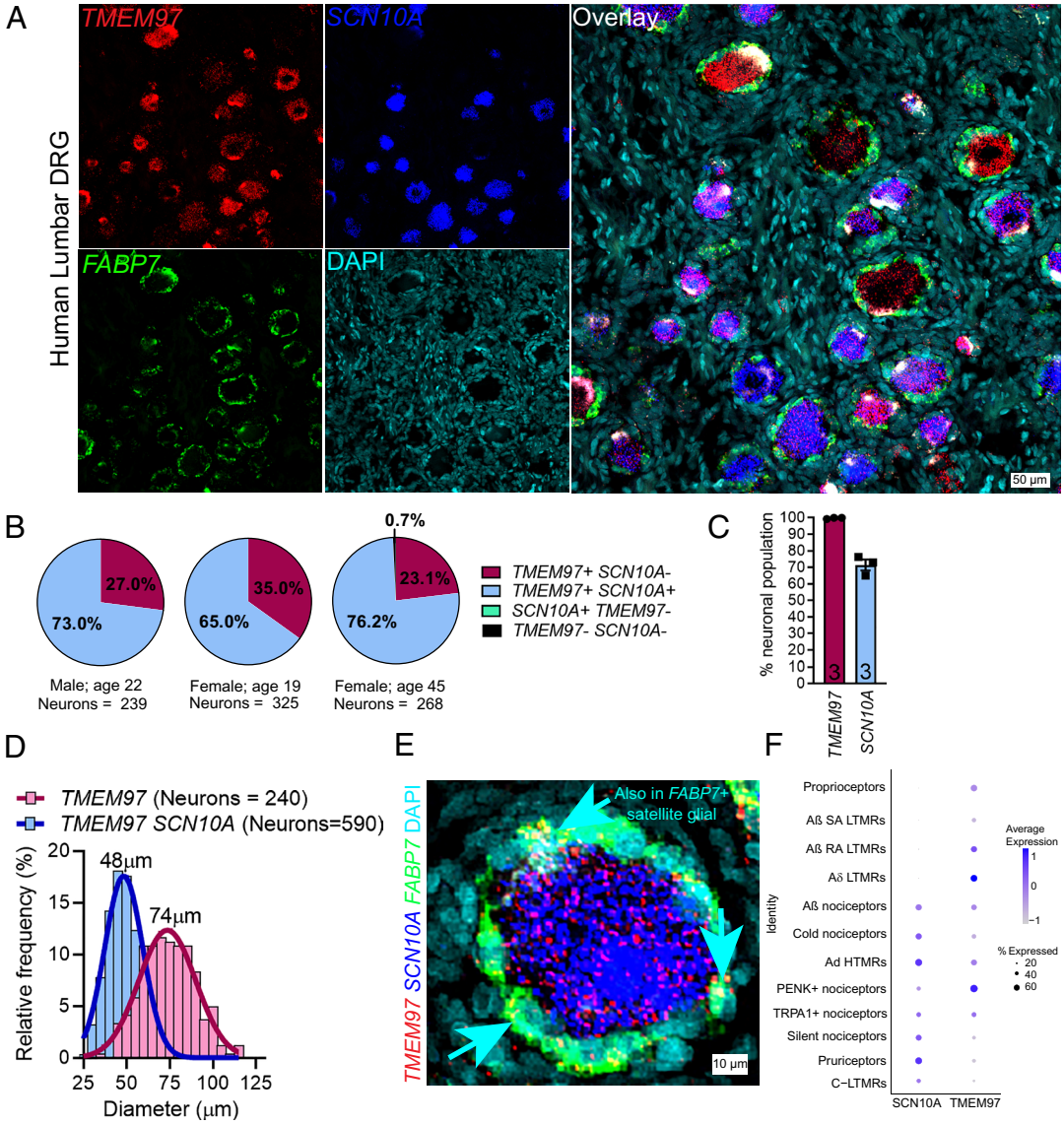

Fig. 1. *TMEM97* gene is expressed in human DRG. (*A*) RNAScope in situ hybridization experiments using lumbar DRGs obtained from organ donors. (*B* and *C*) Across three donors (one male and two females), we found that nearly all DRG neurons (>99%) expressed *TMEM97*, and notably, all *SCN10A*-positive nociceptors expressed *TMEM97*. (*D*) *TMEM97*-positive neurons were distributed across all cell sizes. (*E*) Upon further investigation, we also identified *TMEM97* transcripts in *FABP7*-positive satellite glial cells. (*F*) Our previously published (36) analysis of near single-cell RNA sequencing of human DRGs showed that *TMEM97* is expressed across all neuronal cell types in the ganglia including nociceptors, low-threshold mechanoreceptors (LTMRs), and proprioceptors. *TMEM97* transcripts were notably enriched in proenkephalin (PENK)+ nociceptors and Aδ LTMRs.

Downloaded from https://www.pnas.org by UNIVERSITY OF TEXAS AT DALLAS LIBRARY SERIALS on January 6, 2024 from IP address 129.110.241.53.

of neurons (Fig. 1*D*). Upon further investigation, we found that *FABP7*-positive satellite glial cells also express *TMEM97* (Fig. 1*E*). We identified and quantified *TMEM97*-expressing neuronal subpopulations in the human DRG using our previously published human DRG spatial RNA sequencing dataset (Fig. 1*F*) (36). We validated our findings that *TMEM97* is expressed across all neuronal subtypes in the human DRG with particularly high expression in proenkephalin (PENK)-positive nociceptors and Aδ LTMRs (Fig. 1*F*). Mouse DRG neurons and satellite glial cells express *Tmem97* mRNA (*SI Appendix*, Fig. S1*A*) with a nearly identical pattern to what is seen in the human DRG. Moreover, previously published single-cell RNA sequencing data from mice shows that *Tmem97* is expressed in all DRG neuronal subtypes with particularly high expression in nonpeptidergic neurons, Schwann cells, and satellite glial cells (37). The recently developed harmonized dataset of rodent, nonhuman primate, and human DRGs show that *TMEM97* is expressed in all sensory neuron types (*SI Appendix*, Fig. S1*B*) (38).

Identification of FEM-1689 as a Potent σ_2R/TMEM97 Binding Ligand. Methanobenzazocines and norbenzomorphans represent two distinct chemotypes of biologically active ligands, including UKH-1114, JVW-1034, SAS-0132, and DKR-1677, that bind selectively to σ_2R/TMEM97 (*SI Appendix*, Fig. S2) (39, 40). The first group comprises UKH-1114, which alleviates mechanical hypersensitivity in a mouse model of neuropathic pain (3) and reduces neuronal toxicity in a model of Huntington's disease (20). Based on the positive outcomes using UKH-1114 as a treatment in models of neuropathic pain, we modified its chemical structure to identify less lipophilic analogs with improved binding profiles and physicochemical properties. We synthesized FEM-1689 (*SI Appendix*, Fig. S3), which has one less methylene group than UKH-1114, and found it to be a highly selective compound with improved physicochemical properties (Fig. 2). FEM-1689 is >100-fold more selective for σ_2R/TMEM97 than 40 CNS proteins except for σ_1R (10-fold) and norepinephrine transporter (NET; 24-fold) (*SI Appendix*, Table S1).

Antinociceptive Effect of FEM-1689 in Male and Female Mice Requires an Intact Tmem97 Gene. An important unresolved issue is whether σ_2R/TMEM97 ligands reduce pain hypersensitivity

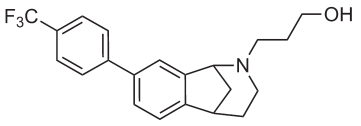

FEM-1689

σ_2R/TMEM97 K_i (nM): 17 ± 8

Highly selective	*Physicochemical properties*	
>100-fold selective for more than 40 CNS proteins except for:	MW	361
	CLogP	4.4
10-fold vs σ_1R (167 ± 54 nM)	tPSA	23.5 Å^2
24-fold vs NET (405 ± 227 nM)	H-bond donors	1
	H-bond acceptors	2
	Rotatable bonds	5

PK properties and brain exposure

T_{max} (IP): 0.5 h (plasma); 2 h (brain)
C_{max} (IP): 508 ng/mL (plasma); 10916 ng/mL (brain)
$t_{1/2}$ (IP): 21.7 h (plasma); 11.4 (brain)
brain to plasma ratio (AUC_{last}): 20.5

Fig. 2. Structure, binding profiles, physicochemical properties, and pharmacokinetic parameters for FEM-1689. Values are reported as averages ± SD.

specifically through action on σ_2R/TMEM97. To address this question, we used a global TMEM97-KO mouse. Male and female TMEM97KO animals and their wild-type counterparts had similar paw mechanical sensitivity (von Frey), paw heat sensitivity (Hargreaves assay), and paw cold sensitivity (acetone) responses suggesting that the loss of TMEM97 did not alter their baseline sensation (*SI Appendix*, Fig. S4). We then examined whether TMEM97KO animals develop an enhanced or blunted mechanical neuropathic pain phenotype following SNI (41) (Fig. 3*A*). Male and female TMEM97KO and wild-type animals developed severe and prolonged mechanical hypersensitivity following SNI when tested at days 7, 10, and 14 after nerve injury (Fig. 3 *B* and *C*). When animals were tested 30 d following nerve injury, they were still mechanically hypersensitive. Male and female wild-type and TMEM97KO animals were then treated with a single intravenous injection of FEM-1689 dosed at 10 mg/kg, a dose determined based on previous studies with the structurally similar σ_2R/TMEM97 ligand, UKH-1114 (3). We assessed TMEM97KO and wild-type evoked mechanical thresholds daily for 7 d and found little or no change for mechanical sensitivity in either group (Fig. 3 *D* and *E*). Animals were allowed to recover for 2 wk before a second treatment with a higher 20 mg/kg dose of FEM-1689. We found that this higher dose effectively reversed mechanical hypersensitivity in both male and female wild-type mice for roughly 4 d with a single administration. Notably, FEM-1689 failed to reduce mechanical hypersensitivity in TMEM97KO mice, showing that the effects of FEM-1689 are dependent on σ_2R/TMEM97. The effect size measurements for FEM-1689 were quantified for males (Fig. 3*F*) and females (Fig. 3*G*).

FEM-1689 Inhibits the ISR and Promotes Neurite Outgrowth in a σ_2R/TMEM97-Dependent Fashion. The next phase of our investigations was directed toward elucidating the mechanism by which FEM-1689 acts on sensory neurons by binding to σ_2R/TMEM97. Prior work has suggested a link between σ_2R/TMEM97 and cholesterol synthesis and trafficking, processes that are heavily regulated by 5′ adenosine monophosphate-activated protein kinase (AMPK) and its substrate, acetyl-CoA carboxylase (42). AMPK agonists are also known to produce antinociception in mouse models (22, 43–46). We treated cultured mouse DRG neurons with FEM-1689 at concentrations covering a range (10, 100, and 1,000 nM), which is consistent with target binding (K_i = 17±8 nM) over the course of 16 h, and found no change in p-ACC levels, whereas A769662 (100 μM), a known AMPK activator, increased p-ACC levels in both wild-type and TMEM97KO neurons (*SI Appendix*, Fig. S5 *A* and *B*). Our observation suggests that FEM-1689 does not influence the AMPK-p-ACC pathway and that a different antinociceptive pathway must be involved.

We then tested the hypothesis that FEM-1689 would inhibit the ISR in DRG neurons. Multiple lines of evidence support this hypothesis: 1) σ_2R/TMEM97 and ISR transducers like protein kinase R-like ER kinase (PERK) are located on the ER membrane (40, 47); 2) a recent report on the effect of 20(*S*)-hydroxycholesterol on σ_2R/TMEM97 implicated the ER-Golgi network (12); and 3) the ISR is engaged in trauma-induced and diabetic neuropathic pain conditions in DRG neurons (25, 26). Accordingly, we cultured mouse DRG neurons from wild-type and TMEM97KO animals, treated them with FEM-1689 over 16 h, and measured changes in the levels of p-eIF2α using immunocytochemistry (ICC) (Fig. 4 *A* and *B*). Measured with ICC, basal levels of p-eIF2α were much lower in TMEM97KO neurons than their wild-type counterparts. Treatment of wild-type neurons with ISRIB (200 nM), a well-known ISR inhibitor, reduced p-eIF2α

Downloaded from https://www.pnas.org by UNIVERSITY OF TEXAS AT DALLAS LIBRARY SERIALS on January 6, 2024 from IP address 129.110.241.53.

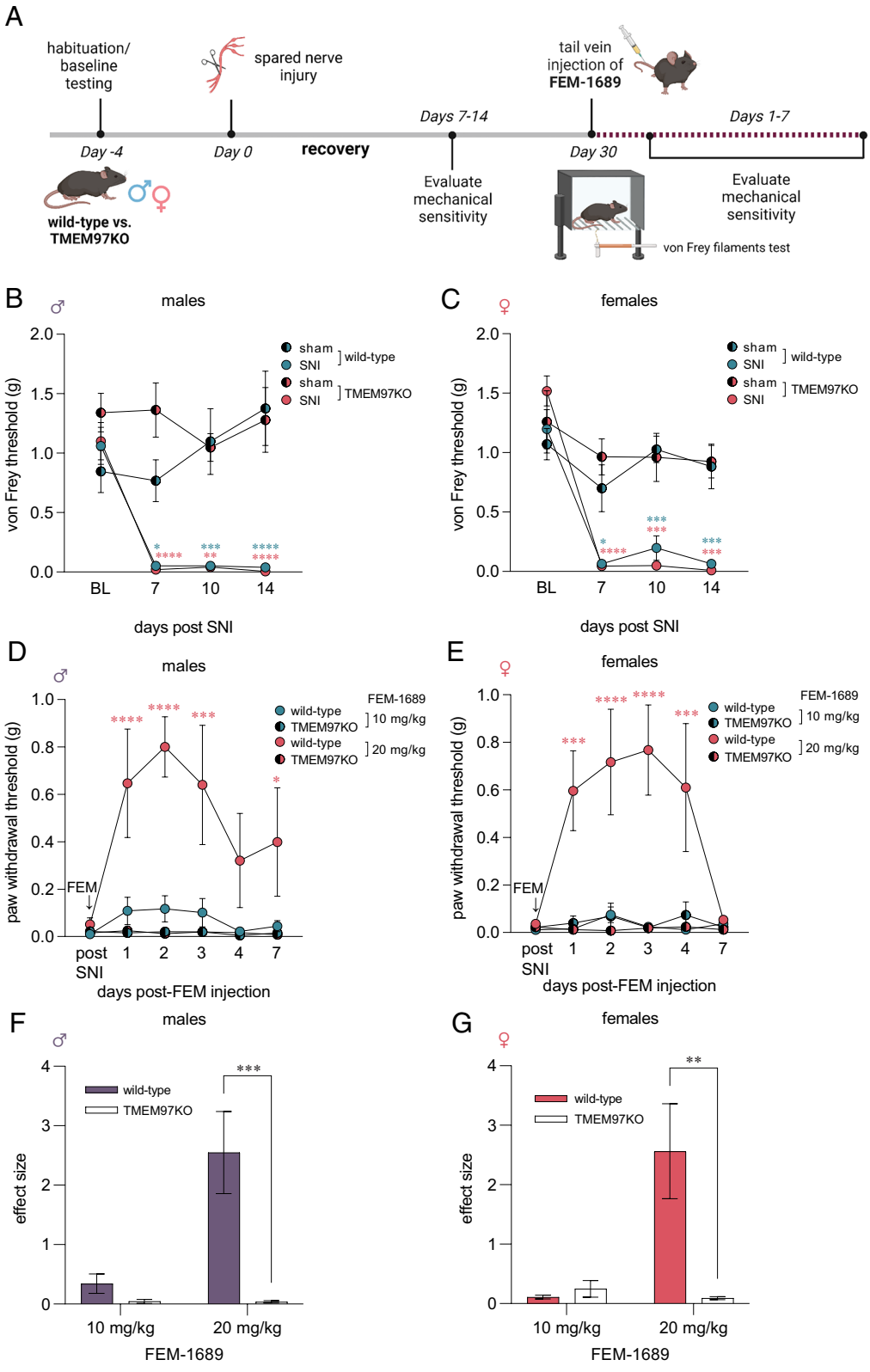

Fig. 3. Mechanical pain hypersensitivity following SNI in wild-type and global TMEM97-KO mice. (*A*) Experimental paradigm. Mechanical hypersensitivity was assessed using the von Frey filaments test at baseline prior to SNI and for 14 d postsurgery. Mice were treated with FEM-1689 (10 mg/kg) intravenously 30 d after SNI surgery and assessed for mechanical hypersensitivity for the following 7 d. Another intravenous injection of FEM-1689 (20 mg/kg) was given 2 wk later and mechanical hypersensitivity assessed for 7 d. (*B* and *C*) Following SNI, no significant difference in mechanical hypersensitivity between wild-type and TMEM97KO littermates of both sexes was observed, suggesting that TMEM97 did not contribute to the development of neuropathic pain following nerve injury. Wild-type SNI (male $n = 6$, female $n = 5$), wild-type sham (male $n = 6$, female $n = 5$), TMEM97KO SNI (male $n = 5$, female $n = 5$), TMEM97KO sham (male $n = 5$, female $n = 5$). (*D* and *E*) A single 20 mg/kg intravenous injection of FEM-1689 reversed mechanical hypersensitivity in wild-type (male $n = 6$, female $n = 5$) but not TMEM97KO (male $n = 5$, female $n = 5$) mice. A lower dose of 10 mg/kg was not sufficient to reduce mechanical hypersensitivity in these animals. Repeated measures two-way ANOVA with Holm-Sidak's multiple comparison test, $^{*}P < 0.05$, $^{**}P < 0.01$, $^{***}P < 0.001$, and $^{****}P < 0.0001$. (*F* and *G*) Effect size analysis demonstrates that a higher dose of 20 mg/kg of FEM-1689 provides maximal antinociceptive effect. Two-way ANOVA with Sidak's multiple comparison test, $^{**}P < 0.01$ and $^{***}P < 0.001$. Blue and red asterisks indicate wild-type and TMEM97KO groups compared to sham controls in (*B* and *C*) and wild-type vs. TMEM97KO groups in (*D* and *E*).

Downloaded from https://www.pnas.org by UNIVERSITY OF TEXAS AT DALLAS LIBRARY SERIALS on January 6, 2024 from IP address 129.110.241.53.

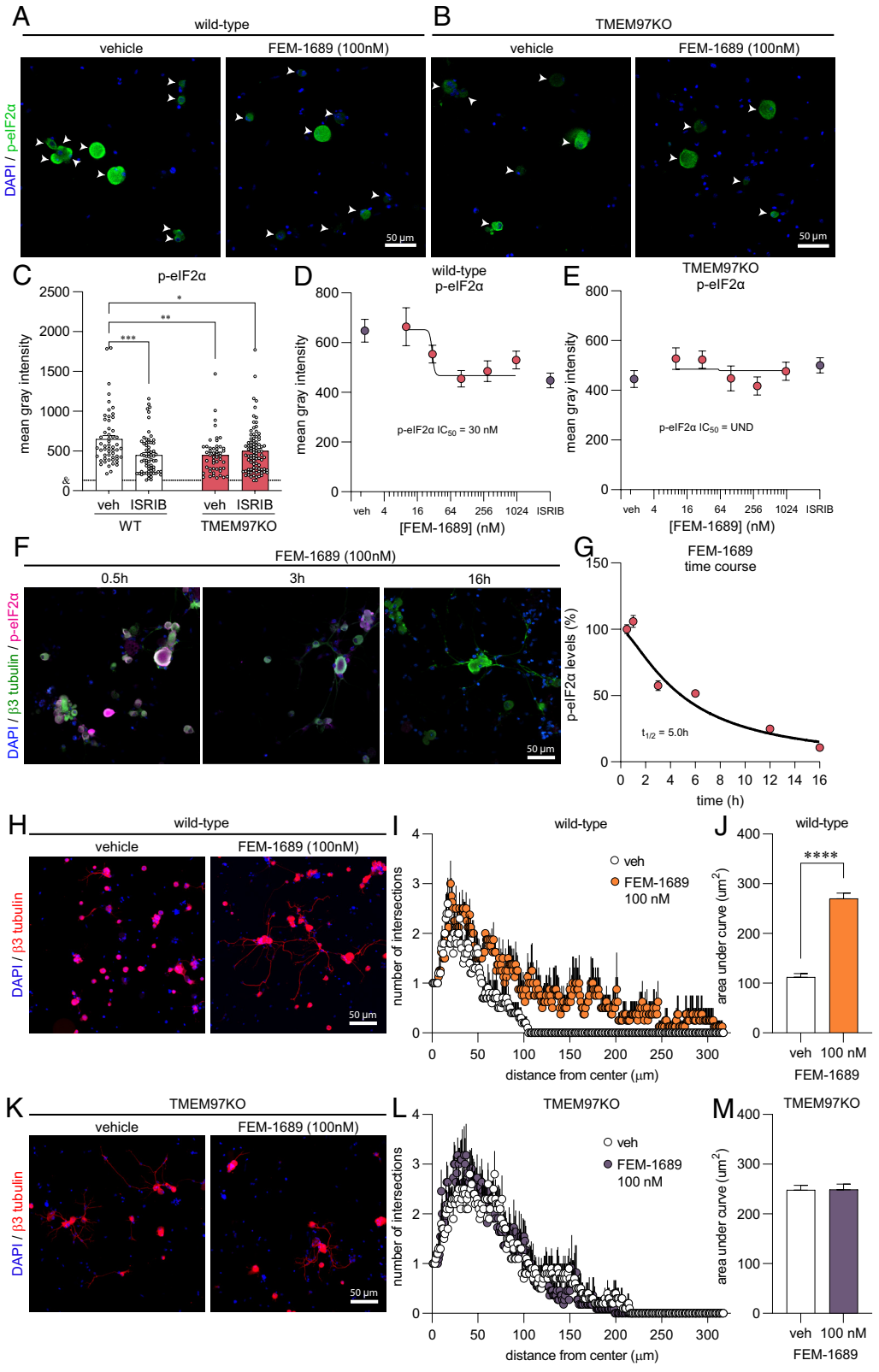

Fig. 4. FEM-1689 reduces p-eIF2α levels and promotes neurite outgrowth in vitro. (*A* and *B*) Cultured mouse DRG neurons obtained from wild-type and TMEM97KO animals were treated with FEM-1689 over 16 h. (*C*) Basal levels of p-eIF2α were lower in TMEM97KO neurons. ISRIB (200 nM) treatment reduced p-eIF2α levels in wild-type neurons but failed to change p-eIF2α immunoreactivity in TMEM97KO neurons. (*D* and *E*) Immunoreactivity of p-eIF2α was assessed across five doses (10, 30, 100, 300 nM, and 1 µM), and a dose–response curve was generated. An IC_{50} of 30 nM was determined with maximal effect at 100 nM which was comparable to ISRIB (200 nM) treatment. TMEM97KO DRG neurons did not respond to FEM-1689 treatment. (*F* and *G*) Wild-type mouse DRG neurons were treated with FEM-1689 (100 nM) at 0.5, 1, 3, 6, 12, and 16 h. We calculated a half-life ($t_{1/2}$) for FEM-1689 of 5.0 h at reducing p-eIF2α levels in vitro. Maximal effect of FEM-1689 was observed at 16 h of treatment. (*H–M*) Sholl analysis of mouse DRG neurons following 100 nM of FEM-1689 treatment showed an increase in the number and complexity of neurites in wild-type neurons but not in TMEM97KO neurons. Area under the curve of Sholl analysis was used to statistically demonstrate this effect. Immunoreactivity against β3-tubulin was used to identify neuronal cell bodies and neurites. Arrows indicate neuronal cell bodies. ***$P < 0.001$ and ****$P < 0.0001$, two-tailed Student's *t* test. UND = undetermined and & = average mean gray intensity of the primary antibody omission control.

Downloaded from https://www.pnas.org by UNIVERSITY OF TEXAS AT DALLAS LIBRARY SERIALS on January 6, 2024 from IP address 129.110.241.53.

levels to the same extent as p-eIF2α levels in vehicle- and ISRIB-treated TMEM97KO neurons (Fig. 4*C*). FEM-1689 reduced p-eIF2α levels, as compared to vehicle-treated cells, in wild-type mouse DRG neurons but not in DRG neurons cultured from TMEM97KO animals (Fig. 4 *D* and *E*). We found that FEM-1689 maximally inhibited the ISR at 100 nM to the same extent as ISRIB (200 nM) (Fig. 4*D*) (48). We calculated the p-eIF2α IC_{50} of FEM-1689 to be 30 nM in wild-type mouse DRG neurons, which was very similar to the binding affinity of FEM-1689 to TMEM97 (K_i = 17 ± 8 nM).

We further characterized the temporal dynamics of FEM-1689 in reducing p-eIF2α levels by treating wild-type mouse DRG neurons with 100 nM FEM-1689 over a time period of 0.5, 1, 3, 6, 12, and 16 h and quantifying immunoreactivity of p-eIF2α (Fig. 4*F*). Using this approach, we calculated a half-life of 5.0 h for FEM-1689 in reducing p-eIF2α levels in vitro. Maximum inhibition of ISR was observed 16 h after treatment of mouse DRG neurons with FEM-1689. This extended time period is consistent with the delayed and prolonged antinociceptive effects of FEM-1689. FEM-1689 did not reduce levels of BiP, a chaperone important for initiating ER stress and ISR, in either wild-type or TMEM97KO neurons (*SI Appendix*, Fig. S5 *C* and *D*). Sholl analysis of cultured mouse DRG neurons showed that FEM-1689 promoted neurite outgrowth in wild-type neurons but not in TMEM97KO neurons (Fig. 4 *F*–*K*). Notably, neurite outgrowth in vehicle-treated TMEM97KO neurons was more pronounced than vehicle-treated wild-type neurons—an observation that may be due to reduced ISR in TMEM97KO cells and hence, enhanced protein synthesis. These data show that σ_2R/TMEM97 is necessary for FEM-1689 to reduce ISR and promote neurite outgrowth.

Norbenzomorphan σ_2R/TMEM97 Ligands SAS-0132 and DKR-1677 Enhance the ISR. The next question we addressed was whether other compounds that bind to σ_2R/TMEM97 inhibit the ISR and whether ISR inhibition is specific to σ_2R/TMEM97 modulators that promote antinociception. We have suggested that dissimilar biological outcomes of σ_2R/TMEM97 modulators may arise from differences in the way individual ligands bind and interact with the protein binding pocket (40). The homologous piperazine-substituted norbenzomorphans SAS-0132 and DKR-1677 (*SI Appendix*, Fig. S2) represent a chemotype that is structurally distinct from the aryl-substituted norbenzomorphan FEM-1689. Computational docking studies of SAS-0132 and FEM-1689, which were performed using the published structure of σ_2R/TMEM97 (4), predict that these two modulators interact differently with the extended binding site of σ_2R/TMEM97 (*SI Appendix*, Fig. S6). SAS-0132, which is neuroprotective but has no antinociceptive effect on its own, was previously shown to inhibit the antinociceptive effects of UKH-1114, which is a homolog of FEM-1689 (3, 17). This observation is consistent with the hypothesis that individual σ_2R/TMEM97 modulators may exert distinct, sometimes opposing, biological effects (3). Indeed, after treatment of wild-type mouse DRG neurons with 10, 30, 100, and 300 nM of SAS-0132 or DKR-1677 over 16 h, we found that both compounds promote the phosphorylation of eIF2α, in contrast to the inhibitory effects of FEM-1689 (Fig. 5). These data suggest that distinct chemotypes of σ_2R/TMEM97 binding compounds have differing effects on the ISR, potentially mediated by how they interact with σ_2R/TMEM97.

FEM-1689 Inhibits the ISR in HEK293T Cells. Human embryonic kidney (HEK) 293 T cells express σ_2R/TMEM97 [The Human

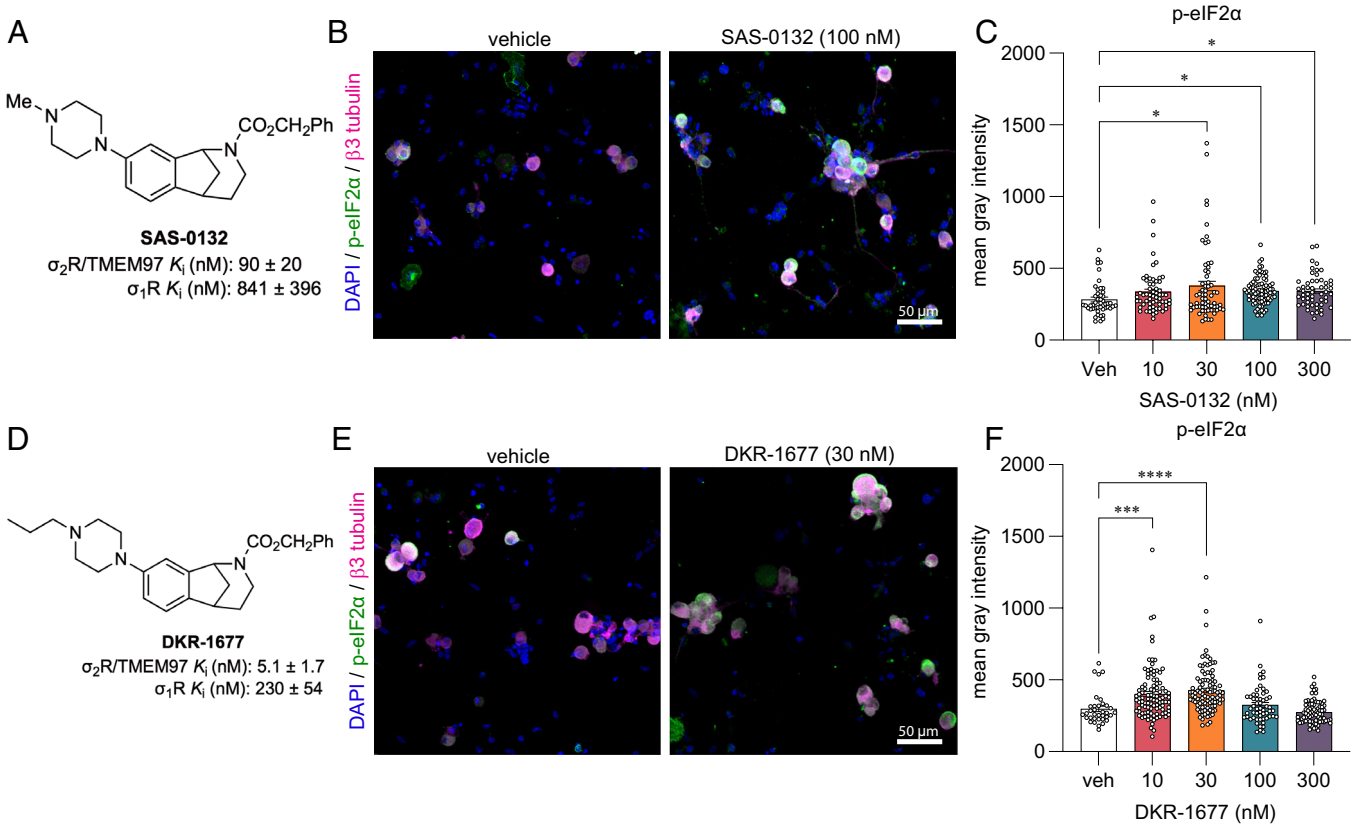

Fig. 5. Norbenzomorphans such as SAS-0132 (*A*–*C*) and DKR-1677 (*D*–*F*) stimulate the ISR by promoting the phosphorylation of eIF2α in cultured wild-type mouse DRG neurons. Cells were treated for 16 h with either SAS-0132 or DKR-1677 at 10, 30, 100, or 300 nM concentrations. Data are presented as fold-change compared to the fluorescence measured in the vehicle-treated neurons. **P* < 0.05, ****P* < 0.001, and *****P* < 0.0001, one-way ANOVA with Tukey's post hoc test.

Downloaded from https://www.pnas.org by UNIVERSITY OF TEXAS AT DALLAS LIBRARY SERIALS on January 6, 2024 from IP address 129.110.241.53.

Protein Atlas (49)], so we queried whether FEM-1689 would inhibit the ISR in this cell line. We found a concentration-dependent reduction in p-eIF2α immunoreactivity following FEM-1689 treatment for either 2 or 16 h using ICC and spectrophotometry (Fig. 6 *A* and *B*). We tested the effect of FEM-1689 over nine concentrations, ranging from 0.1 nM to 1,000 nM, and measured p-eIF2α IC_{50} of FEM-1689 in HEK cells to be 5.9 and 0.7 nM for 2- and 16-h treatment conditions, respectively (Fig. 6 *A* and *B*). We found that the 2-h FEM-1689 incubation period produced a curve with sigmoidal characteristics. We examined the effects of FEM-1689 treatment on a broader panel of ISR-related proteins using western blotting. HEK293T cells treated with FEM-1689 over 16 h showed a concentration-dependent reduction in phosphorylation of eIF2α, eIF2A, and p-PERK, while BiP expression remained stable (Fig. 6 *C*–*K*). Our data show that FEM-1689 influences the PERK-eIF2α arm of the ISR in HEK293T cells and that HEK293 T cells can be used to develop a drug screening platform for pain therapeutics that target σ_2R/TMEM97.

FEM-1689 Reverses Methylglyoxal-Induced Mechanical Hypersensitivity. Methylglyoxal (MGO) is a metabolic by-product of glycolysis that is implicated in diabetic neuropathic pain and other painful neurodegenerative conditions (50–54). We have previously demonstrated that MGO induces an ISR response linked to

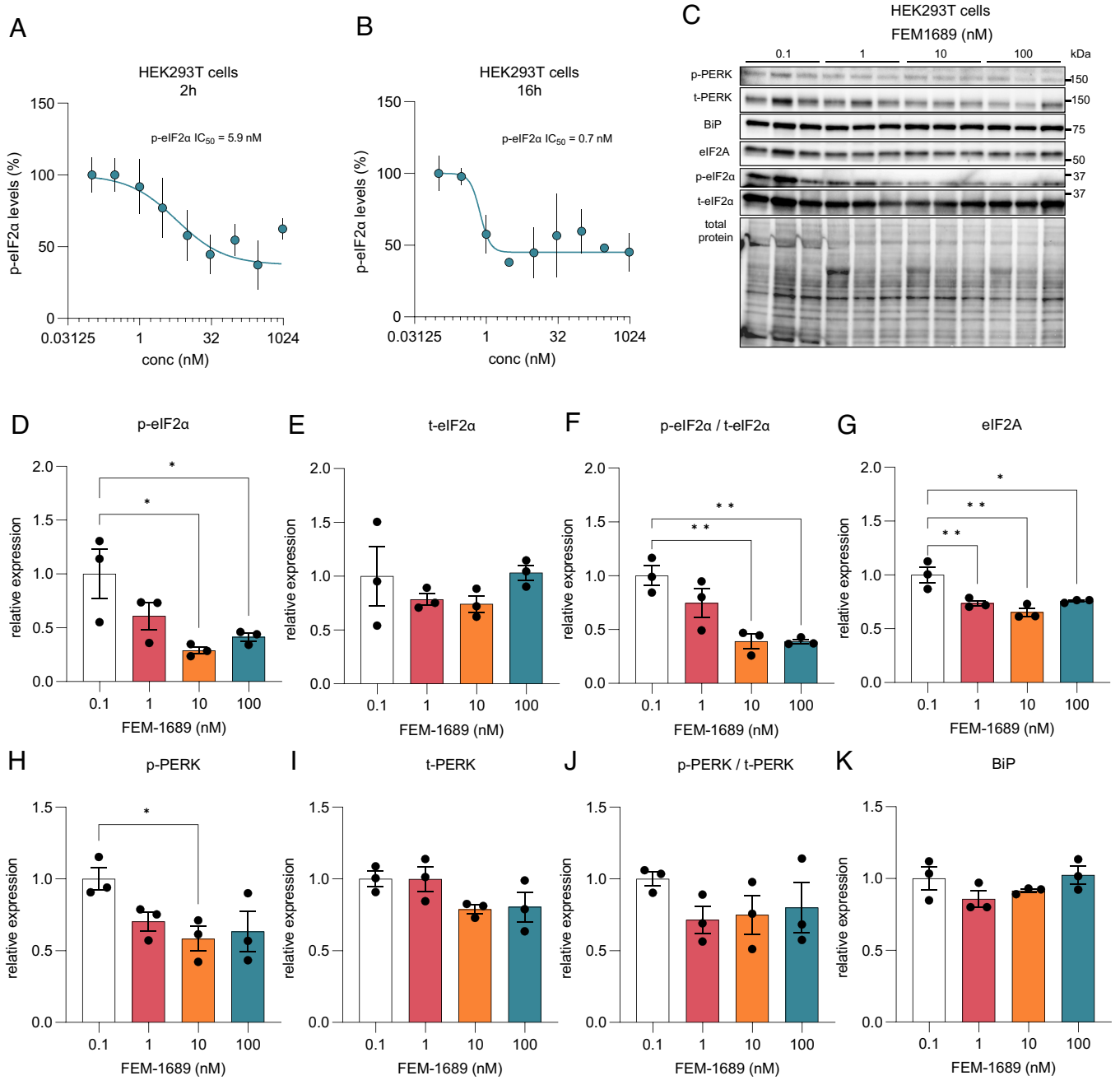

Fig. 6. (*A* and *B*) HEK293T cells were treated for 2 and 16 h with FEM-1689 for across a range of nine concentrations (0.1, 0.3, 1, 3, 10, 30, 100, 300, and 1,000 nM) in 3 to 5 replicates. P-eIF2α levels were measured using ICC and spectrophotometry. IC_{50} was calculated to be 5.89 nM for the 2-h treatment and 0.74 nM for the 16-h treatment. FEM-1689 demonstrated time-dependent effect in reducing p-eIF2α levels in HEK293T cells. (*C*–*K*) In a separate experiment, HEK293T cells treated with FEM-1689 (0.1, 1, 10, and 100 nM) overnight were used for western blot analysis. Western blots showed a significant reduction in p-eIF2α, eIF2A, and p-PERK levels following FEM-1689 treatment suggesting the involvement of the PERK arm of ISR. BiP levels remained unchanged. One-way ANOVA with Tukey's post hoc analysis, $*P < 0.05$ and $**P < 0.01$.

Downloaded from https://www.pnas.org by UNIVERSITY OF TEXAS AT DALLAS LIBRARY SERIALS on January 6, 2024 from IP address 129.110.241.53.

mechanical hypersensitivity in rodents (26). We sought to determine whether the effect of FEM-1689 on reducing levels of p-eIF2α can alleviate ISR-dependent mechanical hypersensitivity caused by MGO. We treated wild-type mice with a single intraplantar injection of MGO (20 ng) to produce mechanical hypersensitivity lasting 6 d (Fig. 7*A*). A group of animals were treated with either FEM-1689 (20 mg/kg, IV) or ISRIB (2.5 mg/kg, intraperitoneal, IP) 24 h following MGO injection. FEM-1689 completely reversed MGO-induced mechanical hypersensitivity over the remaining time course of the experiment whereas the effect of ISRIB was transient (Fig. 7*B*). Our data show that FEM-1689 can completely reverse ISR-dependent pain hypersensitivity caused by MGO, demonstrating the utility for developing σ_2R/TMEM97 modulators for diabetic neuropathic pain.

FEM-1689 Reduces p-eIF2α and Reverses MGO-Induced ISR Activity in Human Sensory Neurons. To extend our findings with rodent DRG findings to humans, we treated cultured human DRG neurons from organ donors with FEM-1689 for 16 h. Consistent with our mouse data, we found that FEM-1689 significantly reduced p-eIF2α levels in human neurons at concentrations of 10 and 100 nM (Fig. 8 *A* and *B*). We then assessed whether FEM-1689 could reverse pathological ISR activation in human DRG neurons. To induce ISR in vitro, we treated human neurons with MGO at 1 μM, a concentration found in the plasma of diabetic neuropathic pain patients (50). MGO treatment increased p-eIF2α levels in human DRG neurons and cotreatment with FEM-1689 (100 nM) prevented this increase (Fig. 8 *C* and *D*). These findings support the conclusion that ISR activation associated with stimuli that cause neuropathic pain in humans can be blocked by σ_2R/TMEM97 modulation.

Discussion

Our experiments clearly demonstrate that the antinociceptive effects of a σ_2R/TMEM97 ligand in mice of both sexes require direct modulation of σ_2R/TMEM97, not σ_1R or any other protein or receptor. This work also shows that modulation of σ_2R/TMEM97 leads to the inhibition of the ISR in mouse and human DRG neurons. Because reduction of the ISR has been linked to pain relief (22, 26, 29), we posit that a plausible cellular mechanism for the antinociceptive effects of FEM-1689 and by extension σ_2R/TMEM97 involves reducing the ISR. Finally, we show that human nociceptors express the *TMEM97* gene, FEM-1689 reduces eIF2α phosphorylation in cultured human DRG neurons, and that the MGO-induced ISR in human neurons can be prevented using FEM-1689. These observations suggest that targeting σ_2R/TMEM97 in pain patients could reduce mechanical hypersensitivity by inhibiting the ISR, a mechanism similarly observed in mice. We conclude that these findings nominate σ_2R/TMEM97 as a bonafide target for developing effective treatments for neuropathic pain.

The time course of action of σ_2R/TMEM97 modulators in mouse neuropathic pain models is different from many other antinociceptive compounds that have a rapid onset of action. Prior to the present study, the slow onset of these antinociceptive effects in the mouse SNI model was independently observed by two different groups using distinct classes of σ_2R/TMEM97 ligands (3, 4). Herein, we have shown that this effect is mediated specifically by σ_2R/TMEM97 because the antinociceptive activity is completely lost in male and female TMEM97KO mice. These observations suggest that the kinetics of signaling for σ_2R/TMEM97 may be the primary underlying reason for the delayed response. The ISR is a major mechanism that controls long-lasting changes in gene expression by influencing the translation of key injury-induced transcription factors like activating transcription factor 4 (ATF4) and C/EBP homologous protein (CHOP). ISR-mediated changes involving multiple transcriptional and posttranslational modifications take time to initiate and progress. It is possible that this time course is responsible for the delay in the onset of action of FEM-1689 vs. the pharmacokinetics of ligand binding to σ_2R/TMEM97. The molecular signaling pathways downstream of σ_2R/TMEM97 modulation require further investigation.

There is an important factor that differentiates other studies of ISR inhibitors and our findings with FEM-1689. In previous studies (26, 29), we noted that ISR inhibitors ISRIB and 4-PBA alleviate mechanical hypersensitivity over a relatively shorter duration of efficacy (hours) in vivo than FEM-1689 (days). The discrepancy in the duration of efficacy of ISRIB and FEM-1689 may be due to differences in their mechanism of action upstream of the ISR pathway as well as the pharmacokinetics of each compound. ISRIB allosterically binds to and promotes the catalytic activity of eIF2B, a guanine nucleotide exchange factor necessary for the recycling of nonphosphorylated eIF2 complex (55–57). In conditions of prolonged and extensive ISR activation, the effects of ISRIB are blunted (58). It is unlikely that FEM-1689 shares the same ISR inhibiting mechanism as ISRIB. So, our

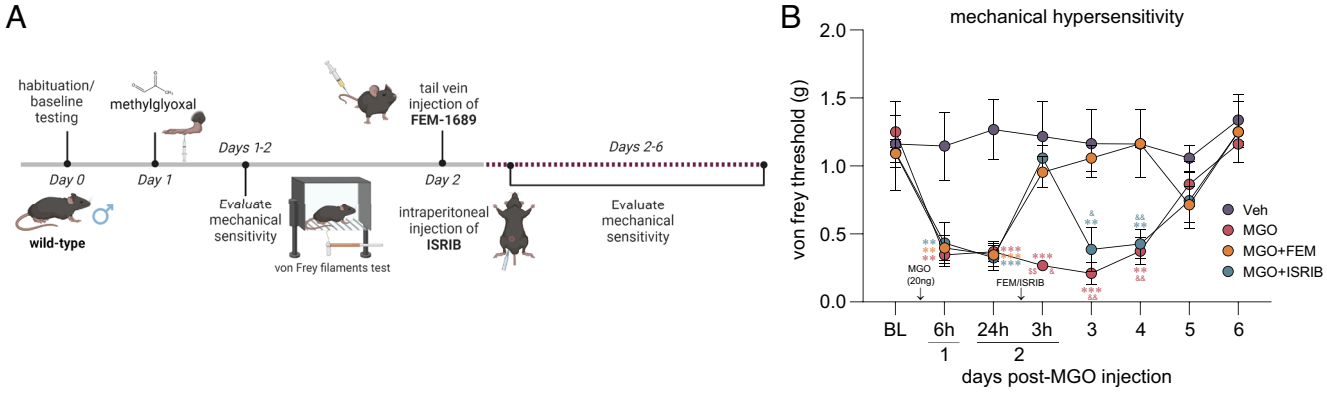

Fig. 7. (*A*) MGO (20 ng) injection in the hind paw induces ISR-dependent mechanical pain hypersensitivity in wild-type mice over a course of 6 d. Mice were treated with FEM-1689 (20 mg/kg, IV) or ISRIB (2.5 mg/kg, IP) 24 h following MGO administration. (*B*) FEM-1689 and ISRIB reversed mechanical hypersensitivity in MGO-treated mice. ISRIB's antiallodynic effects were observed 3 h after drug administration and reverted to a hypersensitive state 24 h after injection. FEM-1689 alleviated mechanical hypersensitivity for the duration of the pain state. **P* < 0.05, ***P* < 0.01, and ****P* < 0.001, repeated measures two-way ANOVA with Tukey's post hoc test. Asterisk (*), dollar sign ($), and ampersand (&) denote post hoc comparison with vehicle (*), MGO+ISRIB ($), and MGO+FEM (&), respectively.

Downloaded from https://www.pnas.org by UNIVERSITY OF TEXAS AT DALLAS LIBRARY SERIALS on January 6, 2024 from IP address 129.110.241.53.

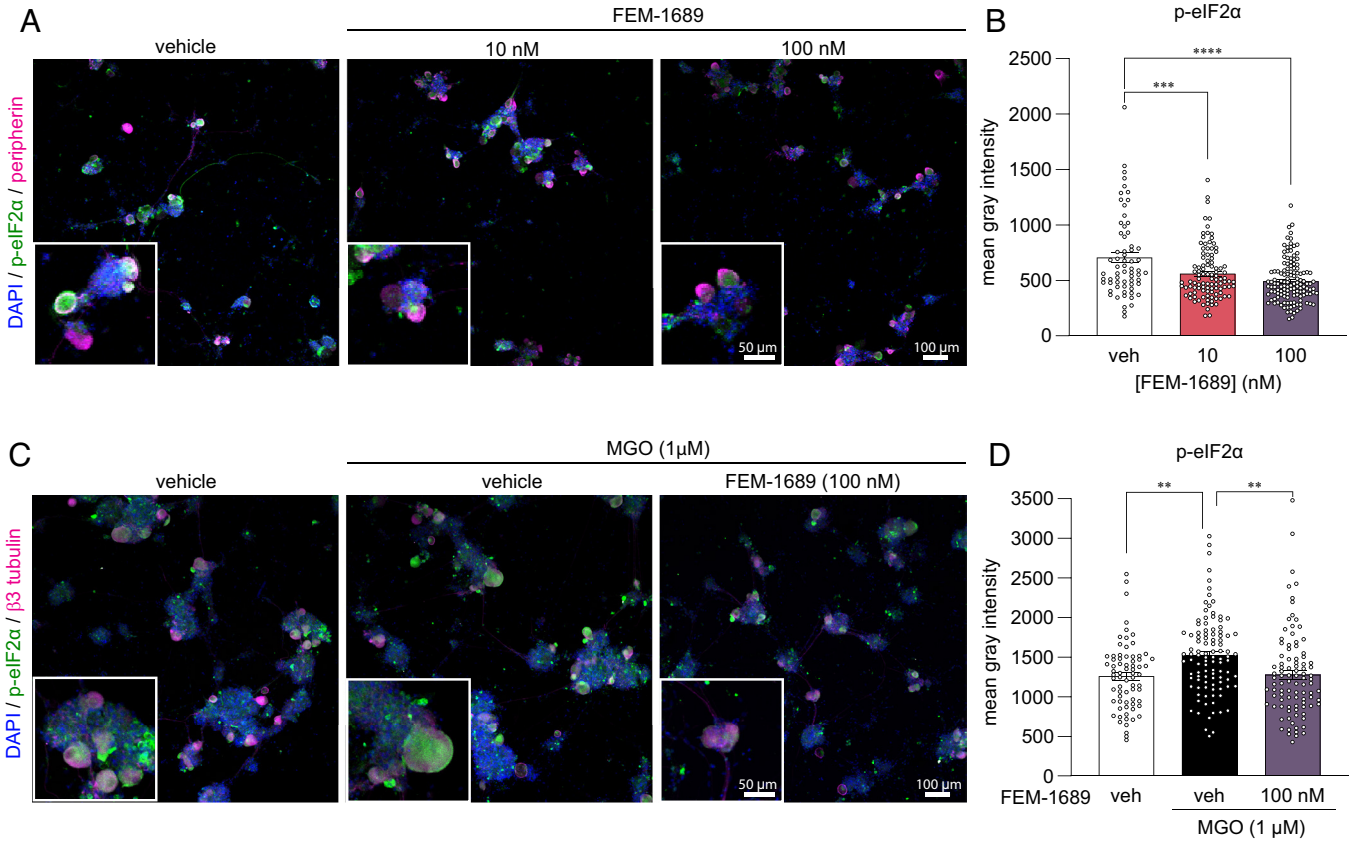

Fig. 8. (*A* and *B*) FEM-1689 treatment (10 and 100 nM) of cultured human DRG neurons significantly reduced p-eIF2α levels. (*C* and *D*) MGO is known to induce the ISR. Cotreatment of human neurons with MGO (1 µM) and FEM-1689 (100 nM) prevented an increase in p-eIF2α suggesting that FEM-1689 limits the effect of MGO. Peripherin and β3-tubulin were used to identify DRG neurons. One-way ANOVA followed by Tukey's post hoc test, $^{**}P < 0.01$, $^{***}P < 0.001$, and $^{****}P < 0.0001$.

observations suggest that FEM-1689 may provide a distinct, more long-term way of modulating ISR than what has been observed previously with ISRIB.

Over the course of our studies to formulate compounds that bind selectively to σ_2R/TMEM97, we have found several chemotypes that exhibit beneficial effects in a number of animal models (40). One group comprises aryl-substituted methanobenzazocines such as UKH-1114 and JVW-1034 (*SI Appendix*, Fig. S2). UKH-1114 alleviates mechanical hypersensitivity following nerve injury (3), and it reduces neuronal toxicity induced by mutant huntingtin protein in a model of Huntington's disease (20). The methanobenzazocine JVW-1034 not only reduces withdrawal behaviors in two rodent models of alcohol dependence (59, 60), but it also alleviates heightened pain sensitivity that is induced by chronic alcohol exposure in mice (60). Herein we report that FEM-1689, a close analog of UKH-1114, also alleviates mechanical hypersensitivity following nerve injury and in response to MGO treatment. Another structural class of σ_2R/TMEM97 modulators include piperazine-substituted norbenzomorphans such as SAS-0132 and DKR-1677 (Fig. 2). For example, SAS-0132 is neuroprotective and improves cognitive performance in animal models of age-related neurodegeneration (17, 61). Notably, SAS-0132 also blocks the antinociceptive activity of UKH-1114 (3), suggesting different σ_2R/TMEM97 binding compounds may have differing effects on nociception. DKR-1677, a homolog of SAS-0132, is protective in two different models of traumatic brain injury (TBI). It reduces axonal degeneration and provides dose-dependent enhancement of cognitive performance in the blast injury model of TBI, while it protects oligodendrocytes and cortical neurons in the controlled cortical impact model (19). DKR-1677 also protects retinal ganglion cells from ischemia/reperfusion injury (21). We demonstrate herein that SAS-0132 and DKR-1677 increase p-eIF2α expression in mouse DRG neurons, whereas FEM-1689 reduces p-eIF2α, suggesting that these compounds have distinct effects on the ISR. These observations provide the basis for developing a drug screening framework for effective pain therapeutics targeting σ_2R/TMEM97.

Understanding how σ_2R/TMEM97 modulators affect the ISR requires further investigation, but there are various clues for direct and indirect influence on the ISR in the literature. First, σ_2R/TMEM97 localization to the ER membrane may link it to the ISR via ER stress, particularly by influencing eIF2α phosphorylation by the kinase PERK. Indeed, we observed a reduction in p-PERK in HEK cells following FEM-1689 treatment at concentrations where p-eIF2α and eIF2A are maximally reduced (Fig. 6), suggesting a possible link between σ_2R/TMEM97 and the PERK pathway. Second, σ_2R/TMEM97 is likely involved in transporting bioactive lipids, such as hydroxycholesterols (12), between cellular compartments, perhaps via a transporter activity like that of Niemann-Pick C1 (NPC1) protein (9). Excessive lipid intake and the demand for increase lipid synthesis promote lipid stress of the ER that is known to activate the PERK-eIF2α branch of the ISR and impair mitochondrial function (62–64). Finally, σ_2R/TMEM97 regulates cellular Ca^{2+} dynamics via its influence on store-operated calcium entry (11). The ER is the largest Ca^{2+} store in the cell and is sensitive to fluctuations in Ca^{2+} levels causing ER stress and ISR induction (65). It is currently unclear whether one or multiple mechanisms linked to inhibition of the ISR are required for antinociception associated with FEM-1689. However, discovery of this link to ISR inhibition enables further exploration

Downloaded from https://www.pnas.org by UNIVERSITY OF TEXAS AT DALLAS LIBRARY SERIALS on January 6, 2024 from IP address 129.110.241.53.

of the downstream mechanistic actions of σ_2R/TMEM97 modulators in DRG neurons.

Neurite outgrowth can be used to assess the neuromodulatory, neuroprotective, and neuroregenerative effects of drugs (66). Our findings demonstrate that FEM-1689 promotes neurite outgrowth and complexity in a σ_2R/TMEM97-dependent manner as measured by Sholl analysis. Neurons lacking σ_2R/TMEM97 also display enhanced neurite outgrowth compared to their wild-type counterparts without any drug treatment. This is explained by a reduced ISR level (Fig. 5*C*), and hence uninhibited protein synthesis in TMEM97KO neurons at basal levels. Axonal growth is a protein synthesis-demanding process so inhibition of the ISR in these conditions is consistent with an enhancement of protein synthesis driving this effect. Previous studies are also consistent with our findings as the ISR inhibitor ISRIB also enhances neurite outgrowth (67). Neuropathic pain models, like SNI, diabetic neuropathy, and chemotherapy-induced neuropathy are characterized by changes in axonal structure in the skin. A recent report demonstrates that aberrant reinnervation of mechanosensitive structures in the skin by nociceptors is a causative factor in late stages of neuropathic pain in mice (68). While we have not assessed skin innervation in the models we have tested, we have previously observed efficacy for σ_2R/TMEM97 modulators in the SNI model at late time points where these skin innervation changes are observed (3). Given the effect we have seen on neurite outgrowth, it will be important to assess whether such effects can be caused in vivo with σ_2R/TMEM97 ligands and whether they can lead to appropriate reinnervation of skin by nociceptors, avoiding aberrant targeting of Meissner's corpuscles that is associated with neuropathic pain (68).

The findings reported herein provide insights regarding the mechanistic origin of the antinociceptive effects that can arise from modulating σ_2R/TMEM97 with small molecules. There remain, however, unanswered questions. First, a definitive link between ISR activation and antinociception in vivo with FEM-1689 must be established. One way to do this would be to evaluate neuropathic pain in *Eif2s1*-KO mice. Such an experiment is complicated because loss of eIF2α, encoded by *Eif2s1*, or completely preventing the phosphorylation of eIF2α through a point mutation is lethal (69). Moreover, no specific antagonists of eIF2α have been described. The widely used classes of compounds that inhibit ISR are chemical chaperones, ISR kinase inhibitors, and eIF2B-stabilizers like ISRIB that do not directly target eIF2α and are not appropriate tools to answer this question. Second, it is unclear why TMEM97KO neurons have less p-eIF2α than WT neurons at baseline. This presents a paradox in which permanent "antagonism" of σ_2R/TMEM97 (i.e., TMEM97KO) and σ_2R/TMEM97 modulation by FEM-1689 both result in a reduction in p-eIF2α levels. This observation may suggest that FEM-1689 sequesters TMEM97 away from its binding partners and prevents the activation of the ISR, producing a KO-like effect. Additionally, the signaling effects of σ_2R/TMEM97-binding compounds may depend on the pathway that is measured, for instance, LDL uptake was reduced to TMEM97KO levels in HeLa cell regardless of whether cells were treated with σ_2R/TMEM97 "agonists" or "antagonists" (8). This was not the case in our observations on p-eIF2α levels. Third, it is important to acknowledge that FEM-1689 may have some polypharmacology as it appreciably binds to σ_1 receptor (Ki = 167 ± 54 nM) and NET (Ki = 405 ± 227 nM), albeit with 10- and 24-fold less potency than σ_2R/TMEM97 (Ki = 17 ± 8 nM). Since the antinociceptive effect of FEM-1689 in TMEM97KO mice is completely abrogated, we conclude that the effect of FEM-1689 in vivo is mediated by σ_2R/TMEM97 and not σ_1 receptor, NET, or other receptors. Moreover, σ_1 receptor antagonists and NET inhibitors alleviate pain hypersensitivity over an acute (hours) or extensively prolonged (days to weeks) time period, respectively, neither of which fit our observations with FEM-1689 (33, 34, 65, 70–73). Nevertheless, at this stage, we cannot rule out the possibility of some polypharmacology with certainty. Fourth, it is important to determine whether the activity of FEM-1689 is due to a peripheral or central site of action. While our pharmacokinetic experiments show that the compound readily enters the brain (Fig. 2), we have also shown that FEM-1689 inhibits the ISR in the DRGs of mice and humans in vitro. Future experiments will use a nociceptor-specific TMEM97 KO mouse under development to address this important issue.

Methods

Animals. TMEM97KO mice were donated by Dr. Liebl (University of Miami, Mouse Resource & Research Centers MMRRC, Tmem97$^{tm1(KOMP)Vlcg}$, stock #050147-UCD) (21). These mice were back crossed with wild-type C57BL/6 mice obtained from Charles River, and a colony was maintained at UTD. More details on the animals used in the study are outlined in *SI Appendix*.

SNI Model of Neuropathic Pain. SNI was performed according to a previously established protocol (3). In short, the peroneal and tibial branches of the nerve were transected and sutured, leaving the sural branch intact. In sham, an incision was made to expose the sciatic nerve, and the wound was closed. More details can be found in *SI Appendix*.

FEM-1689 Intravenous Administration. FEM-1689 was diluted in 100% dimethyl sulfoxide (DMSO, Fisher #67-68-5) to a concentration of 200 mM and stored at −20 °C. It was further diluted in sterile 0.9% saline. The lateral tail vein was injected at 10 mg/kg or 20 mg/kg in 5 μL per gram of mouse (100 μL for a 20-g mouse) using a Hamilton syringe and 27-gauge needle. Animals were anesthetized with isoflurane/oxygen (50:50) during the injection.

Mouse Pain Behavior Assays. Mechanical, cold, and heat sensitivity testing details are outlined in *SI Appendix*.

Mouse Samples: RNAscope In Situ Hybridization. For details regarding mouse RNAscope in situ hybridization experiments, see *SI Appendix*.

Human Samples: DRG Culturing. Human DRG were obtained from organ donors (*SI Appendix*, Table S2) and immersed in ice-cold N-methyl-D-glutamate-supplemented artificial cerebrospinal fluid (as per ref. 74) until enzymatic dissociation. DRG chunks (1 mm) were dissociated in 2 mg/mL STEMzyme I and 4 μg/mL DNAse I (Worthington Biochemical #LS004107, #LS002139) in Hanks' Balanced Salt Solution (HBSS, Gibco #14170161). Tissue was dissociated at 37 °C with trituration using glass pipettes. The dissociated cells were plated on glass coverslips coated with poly-D-lysine (sigma #P7405) and maintained in BrainPhys media (STEMCell #05790) containing 2%SM1 (STEMCell #05711), 1%N2-A (STEMCell #07152), 1%Pen-Strep (ThermoFisher #15070063), and 1%GlutaMax (Gibco #35050061). Further details are outlined in *SI Appendix*.

Human Samples: RNAscope In Situ Hybridization. Fresh frozen human DRGs were embedded in optimal cutting temperature (OCT, TissueTek) and sectioned at 20 μm onto charged slides. RNAScope was performed using the multiplex version 2 kit as instructed by ACDBio and as previously described (75) with slight modifications. Slides were fixed in buffered 10% formalin and dehydrated in 50, 75, and 100% ethanol. A 20-s protease III treatment was used throughout the experiment. Fluorescein β, Cy3, and Cy5 Akoya dyes were used. The probes were *TMEM97* (ACD #554471), *FABP7* (ACD #583891-C2), and *SCN10A* (ACD #406291-C3). RNA quality was assessed for each tissue using a positive control cocktail (ACD #320861). A negative control probe (ACD #320871) was used to check for nonspecific labeling. Images at 40× magnification were acquired on a FV3000 confocal microscope (Olympus) and analyzed using Olympus CellSens. Neuronal diameter was measured using the polyline tool and was drawn across the widest area of the neuronal soma. Lipofuscins were identified as dense bodies of autofluorescence and not analyzed. Only puncta distinct from lipofuscin were analyzed. A positive cell was deemed to have at least one mRNA punctum.

ICC. The ICC protocol was based on a previously published protocol (76). Primary human and mouse cultured cells as well as HEK cells were fixed with 10% formalin for 10 min and then washed three times with PBS (1X). Cells were blocked with 10% normal goat serum (NGS) in PBS-triton X (0.1%). Antibodies were diluted

Downloaded from https://www.pnas.org by UNIVERSITY OF TEXAS AT DALLAS LIBRARY SERIALS on January 6, 2024 from IP address 129.110.241.53.

in an antibody solution (2% NGS and 2% BSA in PBS-triton X). The antibodies used were as follows: p-eIF2α (1:500, Cell Signaling #3398), BiP (1:1000, Cell Signaling #3177), p-ACC Ser79 (1:500, Cell Signaling #3661), β3 tubulin (1:1000, sigma #T8578), peripherin (1:1000, EnCor Biotechnology #CPCA-Peri), and DAPI (1:10,000, Cayman Chemicals #14285). Antibodies were incubated at 4 °C overnight. The primary antibodies were washed with PBS-Tween 20 (0.05%) three times, 10 min each. The secondary antibody Alexa Fluor 488 or Alexa Fluor 555 (Life Technologies, 1:1000) was dissolved in 2% NGS, 2% BSA in PBS-triton X and incubated at room temperature for 1 h. The secondary antibody was washed with PBS-Tween 20 (0.5%) thrice. DAPI was dissolved in PBS and added to the cells for 10 min. It was washed with PBS twice. Each experiment had a primary omission control where the primary antibody was replaced with only the antibody solution to discern any nonspecific binding of the secondary antibody. Coverslips were mounted onto microscope slides and imaged on a confocal. Images were analyzed using Olympus CellSens. Neurons were preferentially selected by their presence of β3 tubulin. ROIs were set to cover the cell soma, and mean gray intensities of each cell were measured. Number of cells analyzed are detailed in *SI Appendix*, Tables S3 and S4.

HEK Cells. Human embryonic kidney (HEK) 293 T cells (ATCC # CRL-3216) were generously donated by the Campbell Lab (UT Dallas). Cells were grown at 37 °C with 5% CO_2 in complete medium (10% FBS, 1% Pen-Strep in DMEM/F12 + GlutaMax (Gibco #10565-018) in T-75 flasks (Greiner Bio-One #658175). In a 96-well plate (ThermoFisher #165305), cells were plated at a density of 20,000 cells per well and grown to roughly 65% confluency before being treated with FEM-1689. For 2-h FEM-1689 treatment, HEK cells were plated at a density of 32,000 cells per well and treated at roughly 85% confluency. Three to five replicates were made per condition/dose (1/2 log steps ranging from 0.1 to 1,000 nM). ICC was performed to label p-eIF2α and DAPI. Immunofluorescence of HEK cells was quantified using the Synergy HTX Multimode Reader. For further details regarding the culturing of HEK cells, see *SI Appendix*.

Mouse Samples: DRG Cultures and Sholl Analysis. Mouse lumbar DRGs were processed and plated as outlined in the human DRG section above with minor differences. Mouse DRG neurons were maintained in DMEM/F12+GlutaMax (Gibco #10565-018) plus 1% Pen-Strep and 1% N2-A. FEM-1689, SAS-0132, and DKR-1677 were dissolved in 100% DMSO and serially diluted in media. Sholl analysis was performed using the Neuroanatomy plugin in ImageJ according to the authors' recommendations (77). Only solitary cells were used for analysis. The area under the curve was calculated using GraphPad Prism. More details are available in *SI Appendix*.

Synthetic Procedures and Characterization. For details regarding FEM-1689 synthesis, binding assays, and docking calculations, see *SI Appendix*.

Data Analysis. All results are presented at mean ± SEM unless stated otherwise. Statistical differences between two groups were determined by two-tailed Student's *t* test. One-way and two-way ANOVAs with repeated measures were used when comparing more than two conditions. Tukey's or Holm-Sidak's post hoc analysis was performed. Specific statistical tests are detailed in figure legends. Statistical significance was set at $P < 0.05$. Data were analyzed and graphed on GraphPad Prism 9.5.1. BioRender was used to build experimental schematics. Effect sizes for FEM-1689 effects on mechanical sensitivity were calculated for each animal and averaged for the group. Effect size = |(baseline-baseline) + (baseline-day1) + … + (baseline-day7)|.

Data, Materials, and Software Availability. All study data are included in the article and/or *SI Appendix*.

ACKNOWLEDGMENTS. This work was supported by Natural Sciences and Engineering Research Council of Canada Postdoctoral Fellowship (M.S.Y.), by NIH grant R01 DK134893 (M.S.Y.), by NIH grant R01 NS0655926 (T.J.P.), and by NIH grant R61 NS127271 (B.J.K.). We are grateful to the organ donors and their families for the gift of life and research provided by their organ donation. We thank Anna Cervantes, Geoffrey Funk, and Peter Horton of the Southwest Transplant Alliance for human tissue recovery. We are grateful to the Robert A. Welch Foundation (F-0652) for funding. We also thank the University of Texas at Austin Mass Spectrometry Facility for high-resolution mass spectral data and the NIH (Grant Number 1 S10 OD021508-01) for funding the Bruker Avance III 500 MHz spectrometer used to characterize synthesized compounds. We are also grateful for the Ki determinations that were generously provided by the National Institute of Mental Health's Psychoactive Drug Screening Program, Contract # HHSN-271-2018-00023-C (NIMH PDSP). The NIMH PDSP is Directed by Professor Bryan L. Roth at the University of North Carolina at Chapel Hill and Project Officer Jamie Driscoll at NIMH, Bethesda, MD.

Author affiliations: [a]Center for Advanced Pain Studies and Department of Neuroscience, School of Behavioral and Brain Sciences, University of Texas at Dallas, Richardson, TX 75080; [b]NuvoNuro Inc., Austin, TX 78712; [c]Department of Chemistry, University of Texas at Austin, Austin, TX 78712; and [d]The Miami Project to Cure Paralysis, Department of Neurosurgery, University of Miami Miller School of Medicine, Miami, FL 33136

1. J. Dahlhamer *et al.*, Prevalence of chronic pain and high-impact chronic pain among adults–United States, 2016. *MMWR Morb Mortal. Wkly Rep.* **67**, 1001–1006 (2018).
2. A. Alon *et al.*, Identification of the gene that codes for the sigma2 receptor. *Proc. Natl. Acad. Sci. U.S.A.* **114**, 7160–7165 (2017).
3. J. J. Sahn, G. L. Mejia, P. R. Ray, S. F. Martin, T. J. Price, Sigma 2 Receptor/Tmem97 agonists produce long lasting antineuropathic pain effects in mice. *ACS Chem. Neurosci.* **8**, 1801–1811 (2017).
4. A. Alon *et al.*, Structures of the sigma2 receptor enable docking for bioactive ligand discovery. *Nature* **600**, 759–764 (2021).
5. G. Cassano *et al.*, F281, synthetic agonist of the sigma-2 receptor, induces Ca^{2+} efflux from the endoplasmic reticulum and mitochondria in SK-N-SH cells. *Cell Calcium* **45**, 340–345 (2009).
6. B. J. Vilner, W. D. Bowen, Modulation of cellular calcium by Sigma-2 receptors: Release from intracellular stores in human SK-N-SH neuroblastoma cells. *J. Pharmacol. Exp. Therap.* **292**, 900–911 (2000).
7. A. Riad *et al.*, The Sigma-2 receptor/TMEM97, PGRMC1, and LDL receptor complex are responsible for the cellular uptake of Aβ42 and its protein aggregates. *Mol. Neurobiol.* **57**, 3803–3813 (2020).
8. A. Riad *et al.*, Sigma-2 receptor/TMEM97 and PGRMC-1 increase the rate of internalization of LDL by LDL receptor through the formation of a ternary complex. *Sci. Rep.* **8**, 16845 (2018).
9. D. Ebrahimi-Fakhari *et al.*, Reduction of TMEM97 increases NPC1 protein levels and restores cholesterol trafficking in Niemann-pick type C1 disease cells. *Hum. Mol. Genet* **25**, 3588–3599 (2016).
10. F. Bartz *et al.*, Identification of cholesterol-regulating genes by targeted RNAi screening. *Cell Metab* **10**, 63–75 (2009).
11. C. Cantonero, P. J. Camello, G. M. Salido, J. A. Rosado, P. C. Redondo, TMEM97 facilitates the activation of SOCE by downregulating the association of cholesterol to Orai1 in MDA-MB-231 cells. *Biochim. Biophys. Acta, Mol. Cell Biol. Lipids* **1866**, 158906 (2021).
12. Y.-S. Cheng *et al.*, A proteome-wide map of 20(S)-hydroxycholesterol interactors in cell membranes. *Nat. Chem. Biol.* **17**, 1271–1280 (2021).
13. Y. S. Huang, H. L. Lu, L. J. Zhang, Z. Wu, Sigma-2 receptor ligands and their perspectives in cancer diagnosis and therapy. *Med. Res. Rev.* **34**, 532–566 (2014).
14. M. Grundman *et al.*, A phase 1 clinical trial of the sigma-2 receptor complex allosteric antagonist CT1812, a novel therapeutic candidate for Alzheimer's disease. *Alzheimers Dement. (N Y)* **5**, 20–26 (2019).
15. N. J. Izzo *et al.*, Alzheimer's therapeutics targeting amyloid beta 1–42 oligomers I: Abeta 42 oligomer binding to specific neuronal receptors is displaced by drug candidates that improve cognitive deficits. *PLoS ONE* **9**, e111898 (2014).
16. N. J. Izzo *et al.*, Alzheimer's therapeutics targeting amyloid beta 1–42 oligomers II: Sigma-2/PGRMC1 receptors mediate Abeta 42 oligomer binding and synaptotoxicity. *PLoS ONE* **9**, e111899 (2014).
17. B. Yi *et al.*, Small molecule modulator of sigma 2 receptor is neuroprotective and reduces cognitive deficits and neuroinflammation in experimental models of Alzheimer's disease. *J. Neurochem.* **140**, 561–575 (2017).
18. C. S. Limegrover *et al.*, Sigma-2 receptor antagonists rescue neuronal dysfunction induced by Parkinson's patient brain-derived α-synuclein. *J. Neurosci. Res.* **99**, 1161–1176 (2021).
19. E. Vazquez-Rosa *et al.*, Neuroprotective efficacy of a Sigma 2 Receptor/TMEM97 modulator (DKR-1677) after traumatic brain injury. *ACS Chem. Neurosci.* **10**, 1595–1602 (2019).
20. J. Jin *et al.*, Neuroprotective effects of σ_2R/TMEM97 receptor modulators in the neuronal model of Huntington's disease. *ACS Chem. Neurosci.* **13**, 2852–2862 (2022).
21. H. Wang *et al.*, σ2R/TMEM97 in retinal ganglion cell degeneration. *Sci. Rep.* **12**, 20753 (2022).
22. M. S. Yousuf, S. I. Shiers, J. J. Sahn, T. J. Price, Pharmacological manipulation of translation as a therapeutic target for chronic pain. *Pharmacol. Rev.* **73**, 59–88 (2021).
23. K. Pakos-Zebrucka *et al.*, The integrated stress response. *EMBO Rep.* **17**, 1374–1395 (2016).
24. E. Zhang *et al.*, Endoplasmic reticulum stress impairment in the spinal dorsal horn of a neuropathic pain model. *Sci. Rep.* **5**, 11555 (2015).
25. O. K. Melemedjian *et al.*, Targeting adenosine monophosphate-activated protein kinase (AMPK) in preclinical models reveals a potential mechanism for the treatment of neuropathic pain. *Mol. Pain* **7**, 70 (2011).
26. P. Barragan-Iglesias *et al.*, Activation of the integrated stress response in nociceptors drives methylglyoxal-induced pain. *Pain* **160**, 160–171 (2019).
27. B. Inceoglu *et al.*, Endoplasmic reticulum stress in the peripheral nervous system is a significant driver of neuropathic pain. *Proc. Natl. Acad. Sci. U.S.A.* **112**, 9082–9087 (2015).
28. S. Lupachyk, P. Watcho, R. Stavniichuk, H. Shevalye, I. G. Obrosova, Endoplasmic reticulum stress plays a key role in the pathogenesis of diabetic peripheral neuropathy. *Diabetes* **62**, 944–952 (2013).
29. M. S. Yousuf *et al.*, Endoplasmic reticulum stress in the dorsal root ganglia regulates large-conductance potassium channels and contributes to pain in a model of multiple sclerosis. *FASEB J.* **34**, 12577–12598 (2020).
30. S. Stone *et al.*, Activating transcription factor 6alpha deficiency exacerbates oligodendrocyte death and myelin damage in immune-mediated demyelinating diseases. *Glia* **66**, 1331–1345 (2018).
31. S. Stone, W. Lin, The unfolded protein response in multiple sclerosis. *Front Neurosci.* **9**, 264 (2015).

Downloaded from https://www.pnas.org by UNIVERSITY OF TEXAS AT DALLAS LIBRARY SERIALS on January 6, 2024 from IP address 129.110.241.53.

32. J. Bruna, R. Velasco, Sigma-1 receptor: A new player in neuroprotection against chemotherapy-induced peripheral neuropathy. *Neural Regen. Res.* **13**, 775–778 (2018).
33. L. Romero, M. Merlos, J. M. Vela, Antinociception by Sigma-1 receptor antagonists: Central and peripheral effects. *Adv. Pharmacol.* **75**, 179–215 (2016).
34. L. Romero *et al.*, Pharmacological properties of S1RA, a new sigma-1 receptor antagonist that inhibits neuropathic pain and activity-induced spinal sensitization. *Br. J. Pharmacol.* **166**, 2289–2306 (2012).
35. B. de la Puente *et al.*, Sigma-1 receptors regulate activity-induced spinal sensitization and neuropathic pain after peripheral nerve injury. *Pain* **145**, 294–303 (2009).
36. D. Tavares-Ferreira *et al.*, Spatial transcriptomics of dorsal root ganglia identifies molecular signatures of human nociceptors. *Sci. Transl. Med.* **14**, eabj8186 (2022).
37. A. Zeisel *et al.*, Molecular architecture of the mouse nervous system. *Cell* **174**, 999–1014.e1022 (2018).
38. S. A. Bhuiyan *et al.*, Harmonized cross-species cell atlases of trigeminal and dorsal root ganglia. bioRxiv [Preprint] (2023). https://doi.org/10.1101/2023.07.04.547740 (Accessed 7 October 2023).
39. J. J. Sahn, T. R. Hodges, J. Z. Chan, S. F. Martin, Norbenzomorphan scaffold: Chemical tool for modulating sigma receptor-subtype selectivity. *ACS Med. Chem. Lett.* **8**, 455–460 (2017).
40. S. F. Martin, Bridging known and unknown unknowns: From natural products and their mimics to unmet needs in neuroscience. *Acc. Chem. Res.* **55**, 2397–2408 (2022).
41. M. Hanner *et al.*, Purification, molecular cloning, and expression of the mammalian sigma1-binding site. *Proc. Natl. Acad. Sci. U.S.A.* **93**, 8072–8077 (1996).
42. D. E. Gordon *et al.*, A SARS-CoV-2 protein interaction map reveals targets for drug repurposing. *Nature* **583**, 459–468 (2020).
43. K. E. Inyang *et al.*, Indirect AMP-activated protein kinase activators prevent incision-induced hyperalgesia and block hyperalgesic priming, whereas positive allosteric modulators block only priming in mice. *J. Pharmacol. Exp. Ther* **371**, 138–150 (2019).
44. K. E. Inyang *et al.*, The antidiabetic drug metformin prevents and reverses neuropathic pain and spinal cord microglial activation in male but not female mice. *Pharmacol. Res.* **139**, 1–16 (2019).
45. K. E. Inyang *et al.*, Alleviation of paclitaxel-induced mechanical hypersensitivity and hyperalgesic priming with AMPK activators in male and female mice. *Neurobiol. Pain* **6**, 100037 (2019).
46. M. D. Burton *et al.*, Pharmacological activation of AMPK inhibits incision-evoked mechanical hypersensitivity and the development of hyperalgesic priming in mice. *Neuroscience* **359**, 119–129 (2017).
47. A. Bertolotti, Y. Zhang, L. M. Hendershot, H. P. Harding, D. Ron, Dynamic interaction of BiP and ER stress transducers in the unfolded-protein response. *Nat. Cell Biol.* **2**, 326–332 (2000).
48. A. A. Anand, P. Walter, Structural insights into ISRIB, a memory-enhancing inhibitor of the integrated stress response. *FEBS J.* **287**, 239–245 (2020).
49. Uhl *et al.*, Tissue-based map of the human proteome. *Science* **347**, 394–394 (2015).
50. A. Bierhaus *et al.*, Methylglyoxal modification of Nav1.8 facilitates nociceptive neuron firing and causes hyperalgesia in diabetic neuropathy. *Nat. Med* **18**, 926–933 (2012).
51. M. M. Dull *et al.*, Methylglyoxal causes pain and hyperalgesia in human through C-fiber activation. *Pain* **160**, 2497–2507 (2019).
52. S. Wetzels, K. Wouters, C. G. Schalkwijk, T. Vanmierlo, J. J. Hendriks, Methylglyoxal-derived advanced glycation endproducts in multiple sclerosis. *Int. J. Mol. Sci.* **18**, 421 (2017).
53. C. C. Liu *et al.*, Accumulation of methylglyoxal increases the advanced glycation end-product levels in DRG and contributes to lumbar disk herniation-induced persistent pain. *J. Neurophysiol.* **118**, 1321–1328 (2017).
54. C. Angeloni, L. Zambonin, S. Hrelia, Role of methylglyoxal in Alzheimer's disease. *Biomed. Res. Int.* **2014**, 238485 (2014).
55. A. F. Zyryanova *et al.*, Binding of ISRIB reveals a regulatory site in the nucleotide exchange factor eIF2B. *Science* **359**, 1533–1536 (2018).
56. A. F. Zyryanova *et al.*, ISRIB blunts the integrated stress response by allosterically antagonising the inhibitory effect of phosphorylated eIF2 on eIF2B. *Mol. Cell* **81**, 88–103.e106 (2021).
57. J. C. Tsai *et al.*, Structure of the nucleotide exchange factor eIF2B reveals mechanism of memory-enhancing molecule. *Science* **359**, eaaq0939 (2018).
58. H. H. Rabouw *et al.*, Small molecule ISRIB suppresses the integrated stress response within a defined window of activation. *Proc. Natl. Acad. Sci. U.S.A.* **116**, 2097–2102 (2019).
59. L. L. Scott *et al.*, Small molecule modulators of sigma2R/Tmem97 reduce alcohol withdrawal-induced behaviors. *Neuropsychopharmacology* **43**, 1867–1875 (2018).
60. S. G. Quadir *et al.*, The Sigma-2 receptor/transmembrane protein 97 (sigma2R/TMEM97) modulator JVW-1034 reduces heavy alcohol drinking and associated pain states in male mice. *Neuropharmacology* **184**, 108409 (2021).
61. S. Mondal *et al.*, High-content microfluidic screening platform used to identify sigma2R/Tmem97 binding ligands that reduce age-dependent neurodegeneration in *C. elegans* SC_APP model. *ACS Chem. Neurosci.* **9**, 1014–1026 (2018).
62. B. F. Teske *et al.*, The eIF2 kinase PERK and the integrated stress response facilitate activation of ATF6 during endoplasmic reticulum stress. *Mol. Biol. Cell* **22**, 4390–4405 (2011).
63. U. I. Onat *et al.*, Intercepting the lipid-induced integrated stress response reduces atherosclerosis. *J. Am. Coll Cardiol.* **73**, 1149–1169 (2019).
64. M. J. Jennings *et al.*, Intracellular lipid accumulation and mitochondrial dysfunction accompanies endoplasmic reticulum stress caused by loss of the co-chaperone DNAJC3. *Front. Cell Dev. Biol.* **9**, 710247 (2021).
65. M. S. Yousuf, A. D. Maguire, T. Simmen, B. J. Kerr, Endoplasmic reticulum-mitochondria interplay in chronic pain: The calcium connection. *Mol. Pain* **16**, 1744806920946889 (2020).
66. S. P. Sherman, A. G. Bang, High-throughput screen for compounds that modulate neurite growth of human induced pluripotent stem cell derived neurons. *Dis. Models Mech.* **11**, dmm031906 (2018).
67. S. K. Young-Baird *et al.*, Suppression of MEHMO syndrome mutation in eIF2 by small molecule ISRIB. *Mol. Cell* **77**, 875–886.e877 (2020).
68. V. Gangadharan *et al.*, Neuropathic pain caused by miswiring and abnormal end organ targeting. *Nature* **606**, 137–145 (2022).
69. A. Khoutorsky *et al.*, eIF2alpha phosphorylation controls thermal nociception. *Proc. Natl. Acad. Sci. U.S.A.* **113**, 11949–11954 (2016).
70. M. S. Yousuf, B. J. Kerr, "Chapter nine–The role of regulatory transporters in neuropathic pain" in *Advances in Pharmacology*, J. E. Barrett, Ed. (Academic Press, 2016), **vol. 75**, pp. 245–271.
71. D. Marks *et al.*, Serotonin-norepinephrine reuptake inhibitors for pain control: Premise and promise. *Curr. Neuropharmacol.* **7**, 331–336 (2009).
72. M. Merlos, L. Romero, D. Zamanillo, C. Plata-Salamán, J. M. Vela, Sigma-1 receptor and pain. *Handb Exp. Pharmacol.* **244**, 131–161 (2017).
73. M. Kremer *et al.*, A dual noradrenergic mechanism for the relief of neuropathic allodynia by the antidepressant drugs duloxetine and amitriptyline. *J. Neurosci.* **38**, 9934–9954 (2018).
74. M. V. Valtcheva *et al.*, Surgical extraction of human dorsal root ganglia from organ donors and preparation of primary sensory neuron cultures. *Nat. Protoc.* **11**, 1877–1888 (2016).
75. S. I. Shiers *et al.*, Convergence of peptidergic and non-peptidergic protein markers in the human dorsal root ganglion and spinal dorsal horn. *J. Comput. Neurol.* **529**, 2771–2788 (2021).
76. M. S. Yousuf *et al.*, Sensory neurons of the dorsal root ganglia become hyperexcitable in a T-cell-mediated MOG-EAE model of multiple sclerosis. *eNeuro* **6**, ENEURO.0024-19.2019 (2019).
77. T. A. Ferreira *et al.*, Neuronal morphometry directly from bitmap images. *Nat. Methods* **11**, 982–984 (2014).

Downloaded from https://www.pnas.org by UNIVERSITY OF TEXAS AT DALLAS LIBRARY SERIALS on January 6, 2024 from IP address 129.110.241.53.